Towards the Automated Design of Metamaterial based Transmission Lines

A. Rodríguez[1], J. Selga[2], J. V. Morro[1], M. Sans[2], F. Martín[2] and V. E. Boria[1]

[1]Instituto de Telecomunicaciones y Aplicaciones Multimedia (iTEAM),
Universitat Politècnica de València,
8G Building - access D - Camino de Vera s/n - 46022 Valencia (Spain)
[2]Centre d'Investigació en Metamaterials per a la Innovació en Tecnologies Electrònica i de Comunicacions (CIMITEC),
Universitat Autònoma de Barcelona,
08193 Bellaterra (Spain)
Corresponding author: amrodri@iteam.upv.es

Abstract

This paper is a review of our work on the automated synthesis and design of artificial transmission lines. Artificial transmission lines based on metamaterial concepts have been a subject of interest in the scientific community during last years. Our line of research is particularly focused on simplifying and accelerating the design of these transmission lines. In the proposed approach, the synthesis is fully automated by the use of space mapping that is a well-known optimization tool in the microwave field. Some of the problems related to the automated synthesis of these lines and how they were solved are outlined in this article. Different examples to illustrate and demonstrate the advantages of this methodology are also presented.

Keywords: artificial transmission lines, space mapping, complementary split ring resonators.

1. Introduction

Transmission lines based on metamaterial concepts can be considered a very interesting alternative to the conventional transmission lines (microstrip, coplanar, etc.) because they present a higher degree of design flexibility, and may offer additional properties as: size reduction [1-2], broadband functionality [2-4], multiband operation [5-6] or spurious suppression [7]. They are implemented by periodically loading a host line with reactive elements (capacitors, inductors, resonators or a combination of them), and they exhibit as a result controllable electromagnetic properties (dispersion or characteristic impedance of the line can be tailored to some extent). However, there is not a systematic methodology for their synthesis, so in general it is a tedious and long process done by the designer, based on the use of EM solvers, equivalent circuit models and parameter extraction procedures. The direct optimization does not properly work (e.g. due to mutual dependence of the parameters involved, the existence of local minima, etc.) and even if it was the case it might be unpractical, because of the computational costs that the EM simulations do usually have (a single possible realization of a complex design has already a high cost). Hence, techniques which avoid direct optimization could be a smart solution to solve this problem. Among the different techniques, space mapping (SM) has been chosen since it is a proven powerful tool in many fields, particularly the microwave field [8-9]. Thanks to the application of SM, specifically the aggressive space mapping (ASM) approach [10], the computational and human cost is dramatically reduced (it does not require special designing skills of the user, and the number of EM simulations is significant smaller).

The paper is organized as follows. First of all, the unit cells synthesized with this methodology are presented. Then, a brief summary of the proposed algorithm, from the formulation of space mapping to the main details of the implementation are given. In section 4, some application examples are presented (including manufactured prototypes and measurements). Finally, most relevant conclusions are outlined.

2. Unit Cells of Study

In the synthesized cells, electrically small planar resonators are used to load a microstrip line. In a first order approximation, the behavior of these small resonators

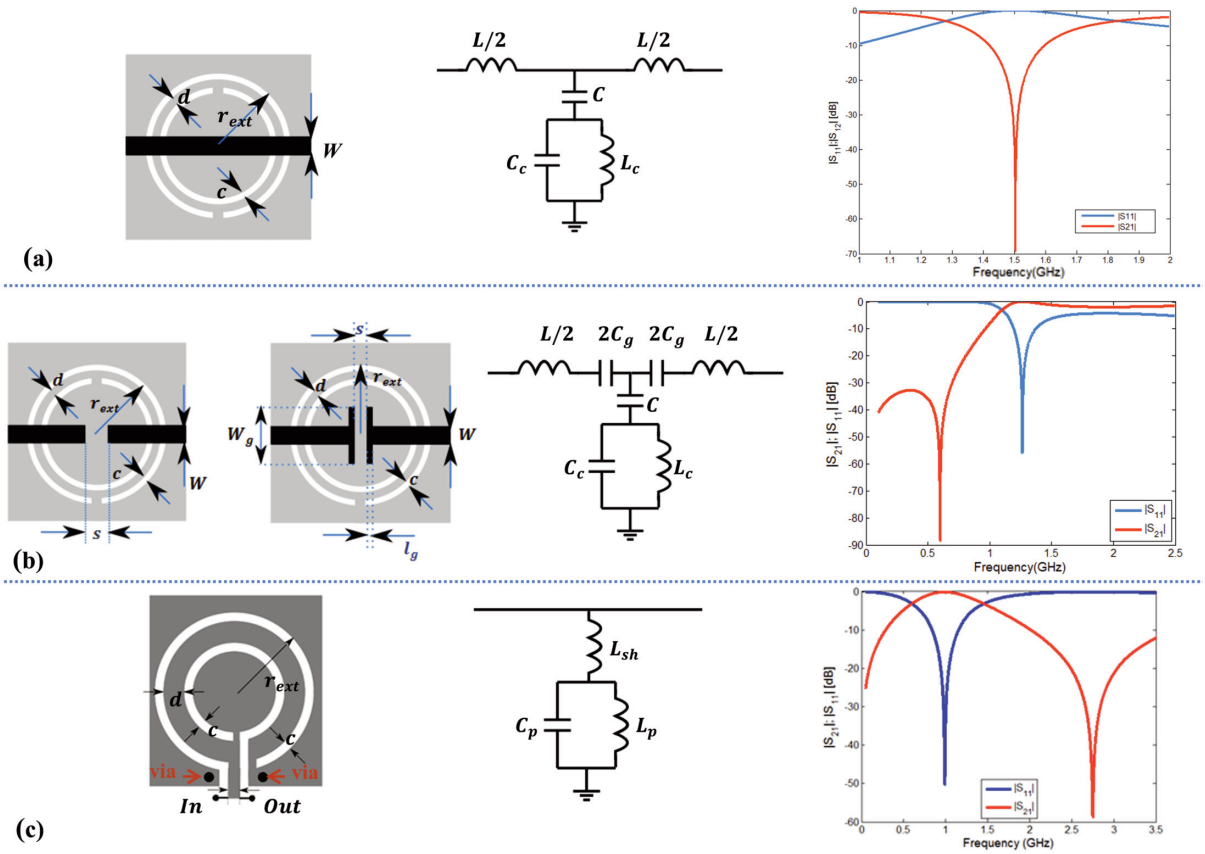

Figure 1. Unit cells (layout, equivalent circuit and typical frequency response): CSRR-loaded microstrip line without series gap (a) and with series gap (b), OCSRR shunt connected to a microstrip line (c).

can be explained in terms of an LC tank. Most widely used resonators in metamaterial field are inspired on the split ring resonator (SRR), proposed by J. Pendry in 1999 [11]. In fact, the first resonant metamaterial transmission line proposed in the literature was SRR-based [12].

The real synthesis of the unit cells presented next is found from their circuit schematics (that provide a given target response), see Fig. 1. The characteristic equivalent circuit model can accurately describe the EM response of every cell in the working region, as it is well studied in [13-14].

The first implemented cell (type 1) consists in a microstrip line with a complementary split ring resonator (CSRR) etched on the ground plane, just beneath the conductor strip as shown in Fig.1.a. With one of these unit cells, or by periodically cascading some of them, a notch (or stop-band) filter can be implemented. The second cell (type 2) is a modification of the previous one which adds a series gap to the host line, see Fig 1.b. Sometimes, instead of using a simple series gap, a T-shaped gap or interdigital capacitor (meander-shaped) is used instead, because they present a bigger capacitance value C_g (modeling the gap) in the equivalent circuit model. The cell exhibits approximately a band-pass or high pass behavior, as shown in Fig. 1.b. The third unit cell example (type 3), is an open complementary split ring resonator (OCSRR) shunt connected to a microstrip line, as illustrated in Fig. 1.c. Due to the inherent transmission zeros associated to the inductance L_{sh} (inductive effect of the metallic strip connecting the resonator to the line), filters which exhibit good stop-band performance can be achieved. By concatenating several unit cells, a wide bandpass filter can be obtained [15].

3. Automated Synthesis

Several problems appeared when we faced the automated synthesis of the different unit cells: determination of the initial layout, initialization of the mapping matrix **B**, parameter extraction procedure implementation, etc. Among them, the most important and challenging one was to guarantee if the target solution could be physically implemented in the chosen technology (permittivity and height of the substrate, technology limits), or in other words if the algorithm can find a realizable solution (converges). To overcome this limitation, a previous stage to the straight implementation (ASM Full-optimization), which basically consists in the identification of a convergence region (CR), was introduced (see Fig. 2).

If the target solution is inside the estimated convergence region (ASM pre-optimization), it means that there is an implementable solution, otherwise the convergence of the algorithm is not guaranteed. The knowledge gained at this stage is used to establish a better initial layout (in-

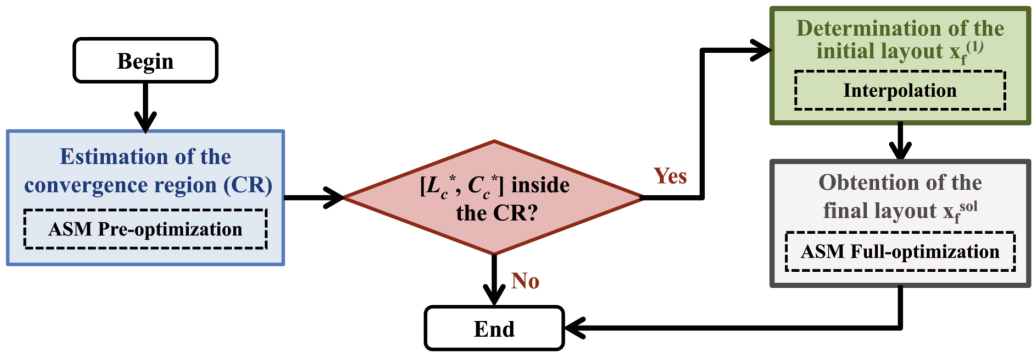

Figure 2. Schematic of two-step aggressive space mapping approach.

terpolation) for the ASM full-optimization, and as a result the second ASM procedure is sped up. In some cases, the new layout is so close to the target, that no further ASM-based optimization is even needed. Since ASM is the core of the algorithm, the conceptual explanation with the basic formulation is provided next (section 3.1).

3.1 Space Mapping Concept and Basic Formulation

The main advantage of SM methods is that the optimization load is shifted from a slow but accurate "fine" model to a fast and less accurate "coarse" model. The algorithm goal, as shows Fig. 3, is to find the function "$\mathbf{P}$" that relates the parameters of the coarse model (denoted by vector $\mathbf{x_c}$), to the parameters of the fine model (denoted by vector $\mathbf{x_f}$). Expressed in a formal language:

$$\mathbf{x_c} = \mathbf{P}(\mathbf{x_f}) \tag{1}$$

such that the corresponding model responses $\mathbf{R_c}$ and $\mathbf{R_f}$ are approximately equal in the region of interest:

$$\mathbf{R_c}(\mathbf{P}(\mathbf{x_f})) \approx \mathbf{R_f}(\mathbf{x_f}) \tag{2}$$

The magnitude of the transfer function (e.g. $|S_{21}|$) is commonly used as the model response for microwave applications.

In the cases of study, a full-wave EM model and the equivalent lumped element circuit model are used as fine and coarse model, respectively. So, if we consider the cell of Fig. 1.a, the corresponding fine model vector is composed by the CSRR external radius (r_{ext}), the separation (d) and width (c) of the slot rings, and also the width of the microstrip line (W): $\mathbf{x_f} = [r_{ext}, c, d, W]$. The length of the strip is approximately set to twice the external radius of the CSRR and the split of the rings is fixed to c. On the other hand, the coarse model vector is defined by the values of the equivalent circuit model elements, *i.e.* $\mathbf{x_c} = [L, C, L_c, C_c]$.

Space Mapping is an iterative process, where a new mapping function $\mathbf{P^{(j)}}$ is estimated at each iteration j. The algorithm converges when the new realization suffices:

$$\left\| \mathbf{R_f}\left(\mathbf{x_f^{(j+1)}}\right) - \mathbf{R_c}(\mathbf{x_c^*}) \right\| < \eta \tag{3}$$

with η a fixed small positive constant ($\eta \longrightarrow 0$), and $\mathbf{x_c^*}$ is the target coarse vector which describes the target solution response. The optimal set of parameters for the fine model is determined by inverting $\mathbf{P^{(j)}}$:

$$\mathbf{x_f^{(j+1)}} = \left(\mathbf{P^{(j)}}\right)^{-1}(\mathbf{x_c^*}) \tag{4}$$

In the aggressive space mapping approach, the solution is found by minimizing the error function $\mathbf{f}$:

$$\mathbf{f}(\mathbf{x_f}) = \mathbf{P}(\mathbf{x_f}) - \mathbf{x_c^*} = 0 \tag{5}$$

If we call $\mathbf{x_f^{(j)}}$ the solution at the *j-th* iteration, the next iterate $\mathbf{x_f^{(j+1)}}$ is obtained:

$$\mathbf{x_f^{(j+1)}} = \mathbf{x_f^{(j)}} + \mathbf{h^{(j)}} \tag{6}$$

where $h^{(j)}$ is the quasi-Newton calculated according to:

$$\mathbf{h^{(j)}} = -\left(\mathbf{B^{(j)}}\right)^{-1}\mathbf{f^{(j)}} \tag{7}$$

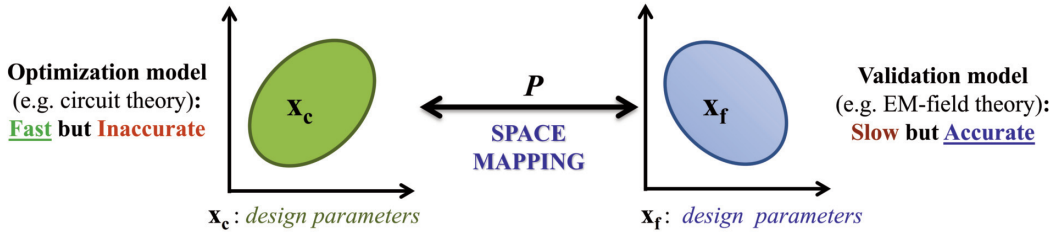

Figure 3. Conceptual Diagram of Space Mapping.

Space Mapping (SM) is a smart way to reduce the computational cost of the optimization process. In the tool proposed (two-step aggressive space mapping) is used in order to:
a) Determine if the target response is implementable (convergence region estimation);
b) Obtain the final topology.

being $\mathbf{B}^{(j)}$ an approximation of the Jacobian matrix $\mathbf{J}$ of the function $\mathbf{f}$ with respect to $\mathbf{x_f}$ at the *j-th* iteration. The mapping matrix $\mathbf{B}^{(j)}$ is properly updated according to the classic Broyden formula as follows:

$$\mathbf{B}^{(j+1)} = \mathbf{B}^{(j)} + \frac{\mathbf{f}^{(j+1)}\mathbf{h}^{(j)T}}{\mathbf{h}^{(j)T}\mathbf{h}^{(j)}} \quad (8)$$

being the super-index T used to denote transpose. Since the calculation of $\mathbf{h}^{(j)}$ requires the inverse of $\mathbf{B}^{(j)}$, it is more convenient to have the same number of parameters in each model, being $\mathbf{B}^{(j)}$ a square non-singular matrix. Therefore, in the application examples if the number of geometrical parameters that define the structure is bigger than the number of circuital parameters of its corresponding equivalent circuit model, some of the physical dimensions are considered as fixed values (e.g. diameter of via) or proportional to other geometrical variables included in the optimization process. Another issue is related to the initialization of $\mathbf{B}$. The classical initialization of the ASM algorithm with the $\mathbf{B}$ matrix equal to the identity is not used, since different kinds of variables are handled (i.e. physical and electrical ones). A numerical derivative based approach (i.e. a finite difference scheme) is used instead, as described in [16].

The algorithm implemented is a constrained version of ASM [17]. Different colors are used in the flow-diagram of Fig. 4, in order to clearly distinguish the different stages involved: initialization (blue), core (black), constrained modification (green). The initial layout, *i.e.* $\mathbf{x_f}^{(1)}$, necessary to start the algorithm is obtained from analytical expressions (based on simple physic approaches) which relate the electrical parameters and the geometrical dimensions for microstrip lines, gaps, small planar resonators, etc. Note that when the next iterate $\mathbf{x_f}^{(j+1)}$ exceeds the acceptable established limits ($\mathbf{x_f}^{min}$ and $\mathbf{x_f}^{max}$), the step $\mathbf{h}^{(j)}$ is decreased in the same quasi-Newton direction by a shrinking factor δ ($0<\delta<1$). Too small dimensions may be impossible to implement due to technological limitations. Moreover, the equivalent circuit model used for the parameter extraction stage might be inaccurate for too extreme dimensions, which is a critical issue for ASM convergence. It is important to remark that in the cases of study, the parameter extraction is a straight forward procedure, meaning that the value of the lumped element of the circuit model are determined directly from the EM simulated response and no additional optimization is needed [14, 16].

The stopping criterion is modified, and instead of using the error function defined in (5), the normalized error function defined for each component *k* as follows:

$$\mathbf{f}_{norm}^{(j)}[k] = \frac{\mathbf{P}(\mathbf{x_f}^{(j)}[k] - \mathbf{x_c}^*[k]}{\mathbf{x_c}^*[k]} \quad (9)$$

is used instead. Then, the norm-2 of the error function $\mathbf{f}_{norm}$ is computed.

3.2 ASM Pre-optimization

The implementable layouts of CSRRs or OCSRRs based lines are limited to certain combinations of the element values of the circuit models (LC tanks). Despite some efforts to establish those limits had been realized in the literature [18], there is not a systematic procedure to determine them. We have proposed a method, consisting on the estimation of a convergence region (values that

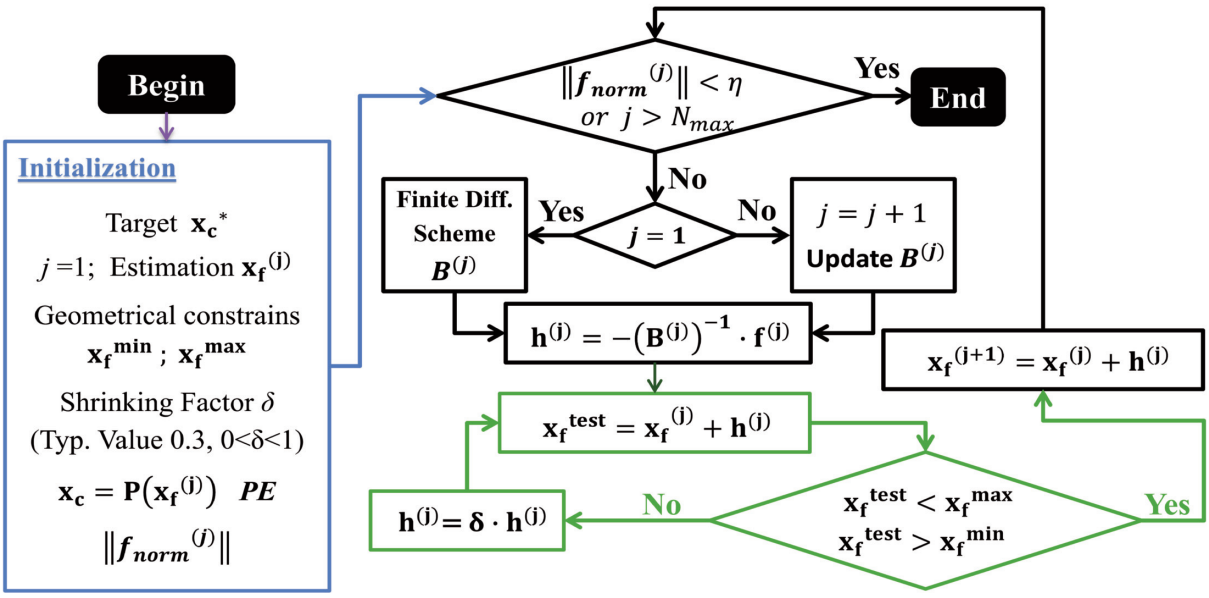

Figure 4. Illustration of the flow-diagram of the ASM algorithm with constrains.

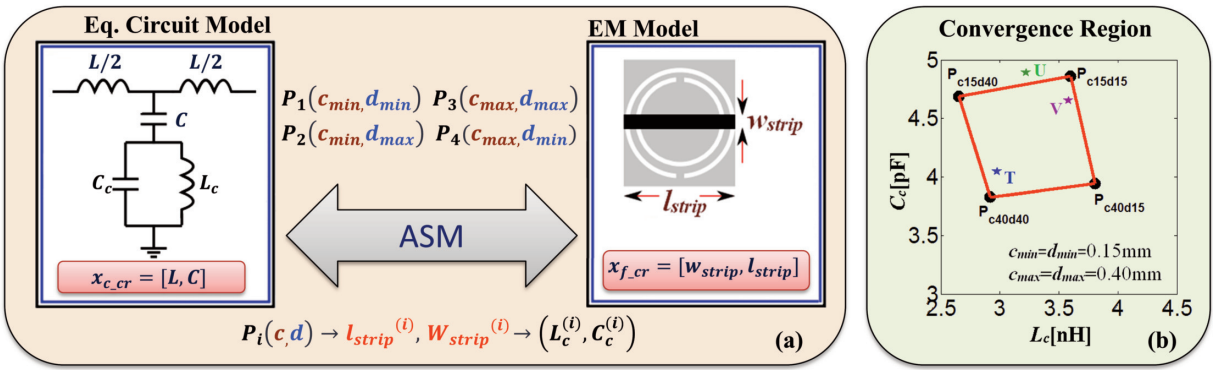

Figure 5. (a) ASM Pre-optimization diagram used to determine the convergence region. (b) Convergence region for a target $\mathbf{x_{c\_cr}}^* = [L^*, C^*] = [5.08\text{nH}, 4.43\text{pF}]$, using as substrate Rogers R03010 (h=1.27mm, ε_r=10.2).

have a practical implementation). This method is explained in detail in [19-21], but a brief explanation for the first case is presented next for completeness.

Taking into account the equivalent circuit model of the unit cell, see Fig. 5.a, the microstrip line is characterized by the parameters L and C. It will be physically implementable as long as these values are not too extreme, and a microstrip line with reasonable width and length results. Hence, given a pair of realizable values for L^* and C^*, a region which determines the implementable circuit values that model the CSRR (L_C,C_C) is calculated by means of ASM. Since the dimensions of the CSRR are the limiting factor, four different scenarios are considered according to the range of acceptable values for the width slot (c_{min} - c_{max}) and for separation between the slots (d_{min} - d_{max}). For each combination of the limiting values of c and d, $P_i(c,d)$, a synthesis solution ($w_{strip}^{(i)}$, $l_{strip}^{(i)}$) providing the requested L^* and C^* values is found. After performing these simple synthesis problems (involving only 2 optimization variables), a set of values for the elements L_C and C_C of the equivalent circuit model are also found. The graphical representation of this set of values gives the desired convergence region corresponding to the target parameters L^* and C^*, see Fig 5.b. The higher number of points to determine the region, the higher accuracy for the convergence region will be. The ASM Pre-optimization process is schematically illustrated in Fig. 5.a (see more details in [19]). With the aim of accelerating the computation of this process, the solution layout calculated for $P_i(c,d)$ is used as the starting point for the next vertex solution (i.e. line dimensions: w_{strip}, l_{strip}).

3.3 ASM Full-Optimization

The second stage is basically the algorithm described in section 3.1, but using an improved initial seed. If we consider that each geometric variable, referred generically as z, is function of L_C and C_C (first order polynomial approximation), the initial layout can be obtained after minimizing the following error by means of a least-squares procedure:

$$\mathbf{f_{error}} = \sum_{j=1}^{N_V} \left(zj - f_{polynomial}\,(L_C\,,\,C_C\,)^2 \right) \qquad (10)$$

where the subscript "j" is the vertex number, and N_V the number of vertexes of the convergence region.

4. Application Examples

As a validation of the proposed design methodology, different application examples have been designed, fabricated and measured. Further details can be found for the first two examples in [20], and for the last one in [22].

4.1 Band-stop filter based on CSRR-loaded transmission lines

A band-stop filter that consists on cascading different unit cells of type 1 (Fig. 1.a), is considered for the first example (3 cells). As it can be seen in Fig. 6, transmission line sections were inserted between adjacent cells (approximately 3/4 of the CSRR external radius) in order to avoid -or minimize- the coupling effects between the adjacent cells that the equivalent circuit used does not take into account.

Since the central frequency of the stop-band is aimed to be 2.45 GHz, the transmission zero frequency (f_z) is set to that frequency value for one cell. The other cells involved in the design will have similar target responses, and therefore very close transmission zero frequencies (i.e. 2.36 GHz and 2.53 GHz). Thus, the optimal coarse solutions for the three cells were forced to be placed in the same convergence region (i.e. with the same target parameters L^* and C^*), as it can be observed in Table 1.

The layouts of the cells obtained following the proposed algorithm are summarized in Table 2, including the number of iterations needed to find the solution with ASM full-optimization and global normalized errors (all under 1%).

The measured filter response (solid black trace), the EM simulated response (green dot-dot-dash line) and the circuital model response (blue dash line) are displayed together for comparison in Fig. 6.c. The measured rejection level is better than 20 dB within a frequency band of 345MHz. These results are in good agreement with the ones predicted by simulation in the band of interest, even

Table 1. - OPTIMAL COARSE SOLUTIONS (UNIT CELLS)

	L[nH]	C[pF]	L_c[nH]	C_c[pF]
$C_{2.36}$	3.194	1.363	1.009	3.143
$C_{2.45}$	3.194	1.363	0.941	3.120
$C_{2.53}$	3.194	1.363	0.882	3.125

Table 2. - FINE PARAMETERS FOR THE FINAL LAYOUTS, ITERATION NO. AND NORMALIZED ERROR

Cell (f_z)	l[mm]	W[mm]	c[mm]	d[mm]	Iter. No.	$\|\|f_{norm}\|\|$
2.36 GHz	5.93	2.16	0.28	0.25	3	0.0074
2.45 GHz	5.91	2.23	0.34	0.27	1	0.0055
2.53 GHz	5.93	2.25	0.34	0.33	5	0.0069

some discrepancies are observed in the out of band frequency range (they can be attributed to fabrication tolerances).

4.2 Dual-band Power Divider based on CSRR-gap-loaded transmission line

The second example is a dual-band power splitter based on a dual-band impedance inverter, implemented by means of a cell of type 2 (Fig. 1.b), as depicted in Fig. 7. To achieve the dual-band functionality, the inverter must provide a phase shift of -90 and +90 degrees at the design operating frequencies, f_1 (0.9 GHz) and f_2 (1.8 GHz), respectively. Therefore, the composite right/left handed behaviour of the structure is exploited, being f_1 located in the left-handed region and f_2 in the right-handed region. As it can be observed in the schematic, two transmission line sections (of characteristic impedance Z_a = 35.35 Ω) were added to the input and output ports of the proposed cell due to practical implementation reasons. The initial calculated element values led to a not implementable solution in that technology (CSRR-based cell), so these values were out of the convergence region. The final target circuital values of the proposed design are summarized in Table 3.

The physical dimensions of the unit cell (CSRR-based with T-shape gap), obtained with the two-step algorithm proposed are collected in Table 4. The width of the line sections is 1.127 mm, corresponding to the indicated characteristic impedance (Z_a) in the considered substrate RO3010. The fabricated prototype is depicted in Fig. 7.b.

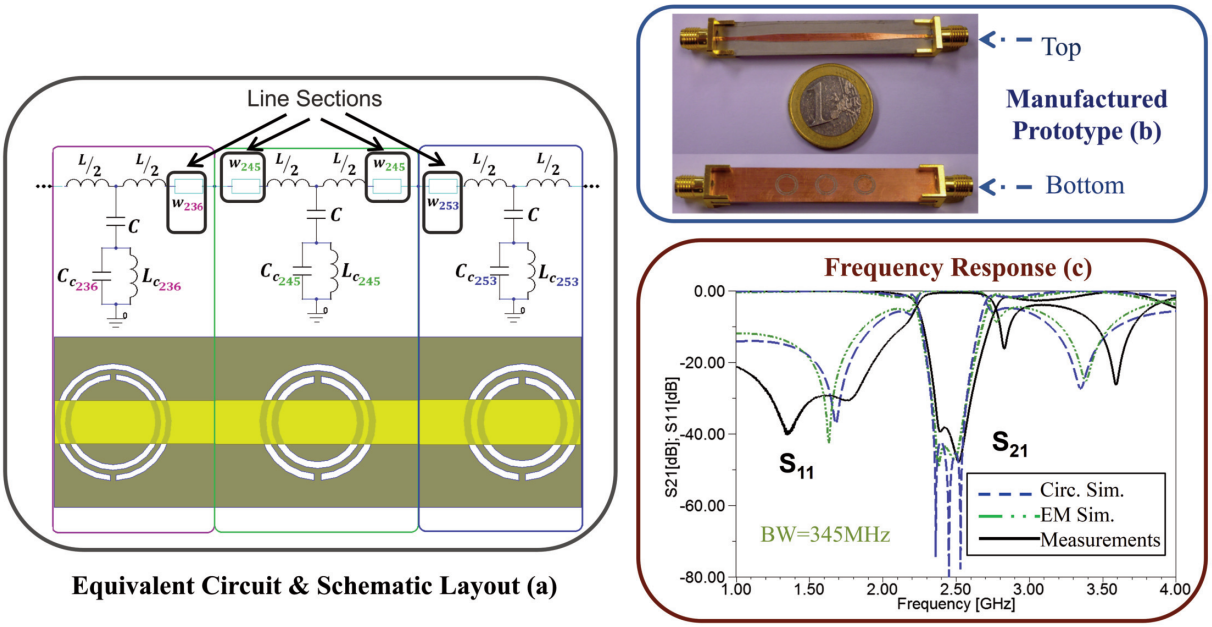

Figure 6. (a) Equivalent circuit and layout of the implementer band-stop filter. (b) Manufactured prototype in Rogers R03010 (h=1.27mm, ε_r=10.2). (c) Magnitude of the scattering parameters S_{21} and S_{11}.

Table 3. - OPTIMAL COARSE SOLUTION

	L[nH]	C[pF]	C_g[pF]	L_c[nH]	C_c[pF]
Target $\mathbf{x_c}^*$	9.45	17.93	1.01	4.85	2.95

Table 4.- FINE PARAMETERS FOR THE FINAL LAYOUT, ITERATION NO. AND NORMALIZED ERROR

	l[mm]	W[mm]	c[mm]	d[mm]	W_g[mm]	Iter. No.	$\|\|f_{norm}\|\|$
CSRR-Cell	5.93	2.16	0.28	0.25	7.13	6	0.0124

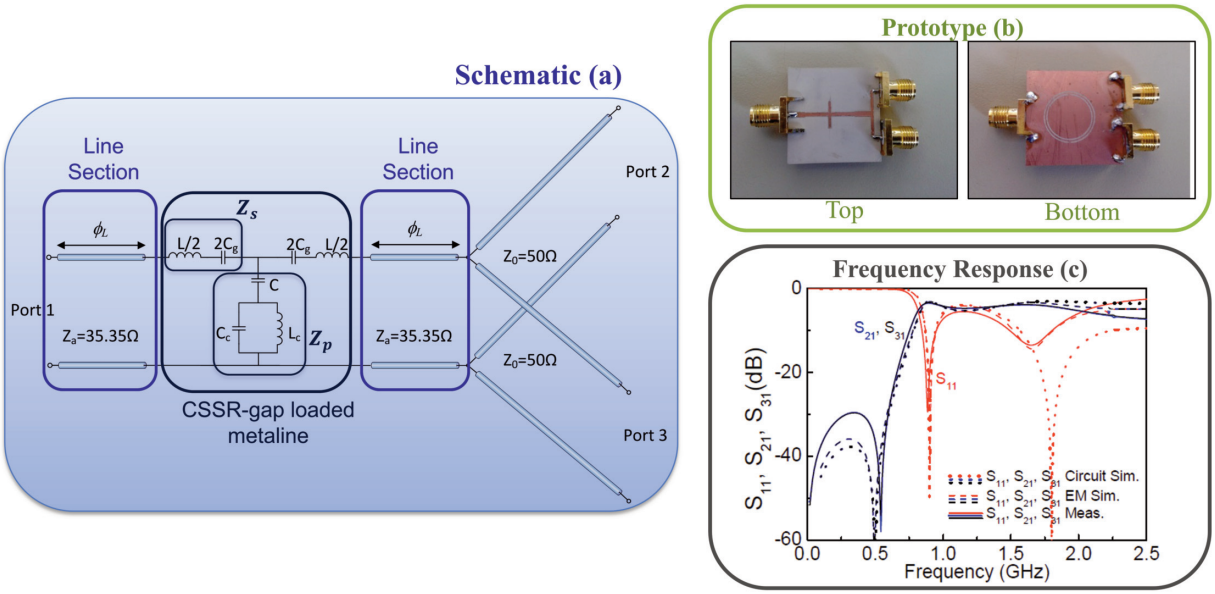

Figure 7. (a) Equivalent circuit of the dual-band power divider prototype. (b) Manufactured prototype in Rogers R03010 (h=0.635 mm, ε_r=10.2). (c) Frequency response of the scattering parameters (in magnitude).

The frequency responses of the synthesized power divider are shown in Fig. 7.c, where optimum matching occurs at f_1 and slightly below f_2. However, the phase shift and the characteristic impedance at f_2 are reasonably close to the nominal values, so it is expected that the functionality of the power divider at that frequency is preserved. The differences observed at high frequencies (in the right-handed band) can be attributed to the coarse model used that is degraded as frequency increases, but not to the proposed design methodology. In order to achieve better results, a more accurate circuit model at high frequencies should be used.

4.3 Bandpass filter based on OCSRR-loaded transmission lines

As final example, a 3-order bandpass filter based on shunt resonators coupled through admittance inverters is presented. The filter layout, is shown in Fig. 8.a, as well as the equivalent circuit where the inverters are already replaced by λ/4 lines (being λ the wavelength at the filter central frequency) of characteristic impedance 50 Ω. The limited functionality of these transmission lines as admittance inverters (narrow band operation) prevents from obtaining the ideal response at the schematic level. Also the ideal response is altered by the transmission zeros related to the inductances L_{shi}, which improve filter selectivity, see section 2. Therefore, the frequency response of the filter roughly corresponds to a 3^{rd}-order Chebyshev bandpass filter with a central frequency f_0=2 GHz, a fractional bandwidth FBW= 30%, and in band ripple of 0.01dB. The calculated target values for a commercial substrate *Rogers RO3010* are summarized in Table 5, as well as the corresponding resonance and transmission zero frequencies.

Using the ASM-based synthesis tool (but in this case without determination of the convergence region), we have determined the dimensions of the OCSRRs cells. Those dimensions are shown, together with the number of iterations needed to synthesize them and the normalized final error (all under 1.3%) in Table 6. The width of the slot rings was fixed to c=0.25 mm, and the dimensions of the strip line that models the λ/4 inverter (electrical length 90º at the central frequency f_0) are w_0= 0.211 mm and l_0 = 14.94 mm.

Table 5.-OPTIMAL COARSE SOLUTIONS, REFLECTION AND TRANSMISSION ZERO FREQUENCIES

	L_p[nH]	C_p[pF]	L_{sh}[nH]	f_0[GHz]	f_z[GHz]
C1, C3	1.813	3.479	0.472	2	4.408
C2	1.143	5.568	0.517	2	3.558

Table 6. - FINE PARAMETERS, ITERATION NO. AND ERROR FUNCTION NORMS

		r_{ext}[mm]	c[mm]	d[mm]	Iter. No.	$\|\|f\|\|$	$\|\|f_{norm}\|\|$
C1, C3	**Initial $x_f^{(1)}$**	4	1.34	0.46	1	8.4542	2.5061
(c=0.20mm)	***Final $x_f^{(6)}$***	2.27	0.95	0.70	6	0.0175	0.0100
C2	***Initial $x_f^{(1)}$***	4	1.01	0.28	1	7.5932	2.6800
(c=0.20mm)	***Final $x_f^{(9)}$***	2.72	1.84	0.75	9	0.0123	0.0122

The agreement between the target (schematic) response and the EM simulation of the synthesized layout is good (losses are not included). In this case, no coupling effects are observed since the unit cells are already sufficiently spaced. However, a spurious band appears due to the fact that the frequency location of the characteristic transmission zeros of the OCSRRs were not considered during the first initial design. The identified spurious band can be avoided by properly designing the OCSRR cells, meaning that all the transmission zeros have to be located at the same frequency.

Recently we have also developed an algorithm able to implement filters automatically, starting directly from filter specifications and not from the circuit schematic as done till now (following aggressive space mapping techniques) [23]. One of the most relevant aspects of this new algorithm is the capability to compensate (in the design stage) the bandwidth reduction and ripple level degradation traditionally caused by the non-ideality of real inverters. In such a reference, a wideband bandpass filter using shunt connecting stepped impedance resonators (SIRs) and grounded stubs coupled through admittance inverters was completely designed following this ASM-based procedures. We have applied similar techniques to other transmission lines based on metamaterial concepts, particularly to the OCSRR-loaded transmission lines considered in the last example, with very good and promising results that have not been published yet.

5. Conclusions and future work

An automated design tool based on aggressive space mapping (ASM) has been proposed and developed. In contrast to other optimization algorithms, we are able to predict whether a given set of element values of the equivalent cir-

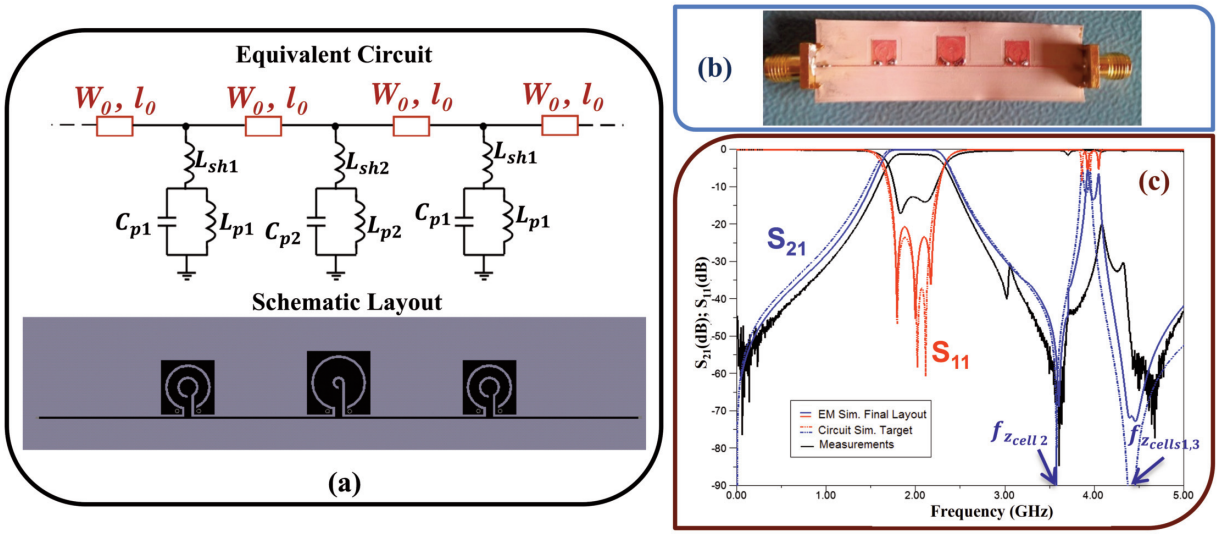

Figure 8. (a) Equivalent circuit and schematic layout of the bandpass filter (b) Manufactured prototype in Rogers R03010 (h=0.254 mm, ε_r=10.2). (c) Frequency response of the scattering parameters (in magnitude).

cuit model of the target unit cell is physically implementable or not (convergence region determination). The main building blocks of the algorithm have been explained. Furthermore, different examples (including manufactured prototypes and measurements) that fully validate the utility and potentiality of the proposed tool have been discussed.

Nowadays we are working towards the application of similar algorithms to other unit cells (e.g. SRRs in coplanar transmission line), other planar technologies (SIRs, slow wave structures, etc.), and more complex designs. Other interesting research line initiated is the development of an unattended automated tools, in other words obtain the physical dimensions of the filter from given specifications.

References

[1] M. Gil, J. Bonache, I. Gil, J. Garcia-Garcia, and F. Martin, "Miniaturization of planar microwave circuits by using resonant-type left-handed transmission lines", IET Microwaves Antennas & Propagation, vol. 1, no. 1, pp. 73-79, Feb. 2007.

[2] J. A. Marcotegui, J. M. Illescas, A. Estevez, and F. Falcone, "Compact ultra wide band microstrip bandpass filter based on multiple-mode resonator and modified complementary split ring resonator", The Scientific World Journal, Nov. 2013.

[3] H. Okabe, C. Caloz, and T. Itoh, "A compact enhanced-bandwidth hybrid ring using an artificial lumped-element left-handed transmission-line section," IEEE Trans. Microw. Theory Techn., vol. 52, no. 3, pp. 798-804, March 2004.

[4] G. Siso, M. Gil, J. Bonache, and F. Martin, "Applications of resonant-type metamaterial transmission lines to the design of enhanced bandwidth components with compact dimensions," Microw. Opt. Technol. Lett., vol. 50, no. 1, pp. 127-134, Jan. 2008.

[5] I. H. Lin, M. DeVincentis, C. Caloz, and T. Itoh, "Arbitrary duad-band components using composite right/left-handed transmission lines," IEEE Trans. Microw. Theory Techn., vol. 52, no. 4, pp. 1142-1149, April 2004.

[6] M. Duran-Sindreu, G. Siso, J. Bonache, and F. Martin, "Planar Multi-Band Microwave Components Based on the Generalized Composite Right/Left Handed Transmission Line Concept," IEEE Trans. Microw. Theory Techn., vol. 58, no. 12, pp. 3882-3891, Dec. 2010.

[7] J. Garcia-Garcia, F. Martin, F. Falcone, J. Bonache, I. Gil, T. Lopetegi, M.A.G. Laso, M. Sorolla and R. Marques, "Spurious passband suppression in microstrip coupled line band pass filters by means of split ring resonators," IEEE Microw. Compon. Lett., vol. 14, no. 9, pp. 416-418, Sept. 2004.

[8] J. W. Bandler, Q. Cheng, S.A. Dakroury, A. S. Mohamed, M. H. Bakr, K. Madsen, and J. Søndergaard, "Space mapping: The state of the art," IEEE Trans. Microw. Theory Techn., vol. 52, no. 1, pp. 337–361, Jan. 2004.

[9] S. Koziel, Q. S. Cheng and J. W. Bandler, "Space mapping," IEEE Microwave Magazine, vol.9, no. 6, pp.105-122, Dec. 2008.

[10] J.W. Bandler, R.M. Biernacki, S.H. Chen, R.H. Hemmers and K. Madsen, "Electromagnetic optimization exploiting aggressive space mapping," IEEE Trans. Microw. Theory Techn., vol. 43, no. 12, pp. 2874-2882, Dec. 1995.

[11] J. B. Pendry, A. J. Holden, D. J. Robbins, W. J. Stewart, "Magnetism from conductors and enhanced non-linear phenomena," IEEE Trans. Microw. Theory Techn., vol. 47, pp. 2075-2084, Nov. 1999.

[12] F. Martín, F. Falcone, J. Bonache, R. Marques and M. Sorolla, "A new split ring resonator based left handed coplanar waveguide", Applied Physics Letters, vol. 83, no. 22, pp. 4652-4654, Dec. 2003.

[13] J. D. Baena, J. Bonache, F. Martin, R. M. Sillero, F. Falcone, T. Lopetegi, M. A. G. Laso, J. Garcia-Garcia, I. Gil, M. F. Portillo, and M. Sorolla, "Equivalent-circuit models for split-ring resonators and complementary split-ring resonators coupled to planar transmission lines," IEEE Trans. Microw. Theory Techn., vol. 53, no.4, pp. 1451-1461, April 2005.

[14] F. Aznar-Ballesta, M. Gil, M. Duran-Sindreu, J. Bonache and F. Martín "Characterization of metamaterial transmission lines with coupled resonators through parameter extraction", Metamaterial, Dr. Xun-Ya Jiang (Ed.), chapter 12, pp. 303-320, InTech, May 2012.

[15] P. Velez, J. Naqui, M. Duran-Sindreu, J. Bonache, and F. Martín, "Broadband microstrip bandpass filter based on open complementary split ring resonators," Int J Antennas Propag., article ID 174023, pp. 1-6, Oct. 2012.

[16] A. Rodriguez, J. Selga, F. Martin, and V. E. Boria, "Practical Application of Space Mapping Techniques to the Synthesis of CSRR-Based Artificial Transmission Lines", in Surrogate-Based Modeling and Optimization, S. Koziel and L. Leifsson (Editors), New York, Springer, pp. 81-97, 2013.

[17] J.E. Rayas-Sanchez and V. Gutiérrez-Ayala, "EM-based Monte Carlo analysis and yield prediction of microwave circuits using linear-input neural-output space mapping," IEEE Trans. Microw. Theory Techn., vol. 54, pp. 4528–4537, Dec. 2006.

[18] J. Bonache, M. Gil, O. Garcia-Abad, and F. Martin, "Parametric analysis of microstrip lines loaded with complementary split ring resonators," Microw. Opt. Technol. Lett., vol. 50, no. 8, pp. 2093-2096, Aug. 2008.

[19] A. Rodriguez, V. E. Boria, J. Selga, and F. Martin, "A robust space mapping method for the practical synthesis of CSRR-based artificial transmission lines from equivalent circuit models", in Proc. EuMC2012, Amsterdam (The Netherlands), pp. 671-674, Nov. 2012.

[20] J. Selga, A. Rodriguez, V. E. Boria, and F. Martin, "Synthesis of split rings based artificial transmission lines through a new two-step, fast converging, and robust Aggressive Space Mapping (ASM) algorithm", IEEE Trans. Microw. Theory Techn., vol. 61, no. 6, pp. 2295-2308, June 2013.

[21] J. Selga, A. Rodriguez, M. Orellana, V. E. Boria, and F. Martin, "Automated synthesis of transmission lines loaded with complementary split ring resonators (CSRRs) and open complementary split ring resonators (OCSRRs) through aggressive space mapping (ASM)," Applied Physics A, vol. 117, issue 2, pp. 557-565, Nov. 2014.

[22] A. Rodriguez, J. Selga, V. E. Boria, and F. Martin, "Synthesis of open complementary split ring resonators (OCSRRs) through aggressive space mapping (ASM) and application to bandpass filters", Proceedings of 44th European Microwave Conference (EuMC), Rome (Italy), pp. 323-326, 0ct. 2014.

[23] M. Sans, J. Selga, A. Rodriguez, V. E. Boria, and F. Martin, "Unattended synthesis of planar wideband bandpass filters from specifications using a two-step aggressive space mapping (ASM) algorithm," IEEE Trans. Microw. Theory Techn., vol.62, no.12, pp. 3341-3350, Dec. 2014.

Biographies

Ana Rodriguez (S'10-M'15) was born in Lugo, Spain. She received the Telecommunications Engineering degree from the Universidade de Vigo (UV), Spain, in 2008. As a student, she participated in the Erasmus exchange program, developing the Master Thesis at the University of Oulu, Finland. Since the end of 2008, she has joined the Institute of Telecommunications and Multimedia Applications (iTEAM), which is part of the scientific park at the Universitat Politècnica de València (UPV), Spain. She obtained "Master en Tecnología, Sistemas y Redes de Comunicaciones" and "Doctor Ingeniero de Telecomunicación" degrees from the Universidad Politécnica de Valencia, in 2010 and 2014, respectively. Her main research interests include CAD design of microwave devices, EM optimization methods and metamaterials.

Jordi Selga (S'11-M'14) was born in Barcelona, Spain, in 1982. He received the B.S. Degree in Telecommunications Engineering - Electronic Systems in 2006, the M.S. Degree in Electronics Engineering in 2008 and the PhD degree in Electronics Engineering in 2013 from the Universitat Autònoma de Barcelona (UAB), Barcelona, Spain. Since 2008 is member of CIMITEC-UAB, a research centre on Metamaterials supported by TECNIO (Catalan Government). He was holder of a national research fellowship from the Formación de Profesorado Universitario Program of the Education and Science Ministry (Reference AP2008-4707). He is currently working in subjects related to metamaterials, CAD design of microwave devices, EM optimization methods and automated synthesis of planar microwave components at the UAB.

José V. Morro (S'02-M'10) was born in Segorbe (Castellón), Spain, in 1978. He received his "Ingeniero de Telecomunicación" and "Doctor Ingeniero de Telecomunicación" degrees from the Universidad Politécnica de Valencia, Valencia, Spain, in 2001 and 2011, respectively. In 2001, he became a Research Assistant in the Universidad Politécnica de Valencia. In 2003 he joined the "Area de Teoría de la Señal y Comunicaciones", Universidad Miguel Hernández de Elche, where he served as a Lecturer (2003-2005). In 2005 he rejoined the "Departamento de Comunicaciones", Universidad Politécnica de Valencia, where he serverd as an Assistant Lecturer (2005-2007) and now he is Lecturer (since 2007). His current research interests are focused on the synthesis and automated design of passive components in waveguide, planar and hybrid technologies, and on left-handed structures.

Marc Sans was born in Terrassa (Barcelona), Spain, in 1982. He received the B.S. Degree in Telecommunications Engineering - Electronic Systems in 2006, the M.S. Degree in Telecommunications Engineering in 2008 and the M.S. Degree in Electronics Engineering in 2013 from the Universitat Autònoma de Barcelona (UAB). In 2008 he started his professional career as a RF Engineer at Sony-FTVE developing the RF stage of TV receivers. In 2010 he moved to Mier Comunicaciones S.A. to carry out the design of passive and active devices for VHF-UHF broadcasting units. Since 2014 he is working towards the PhD Degree at CIMITEC-UAB in the synthesis of microwave devices based on EM optimization techniques.

Ferran Martín (M'04-SM'08-F'12) was born in Barakaldo (Vizcaya), Spain in 1965. He received the B.S. Degree in Physics in 1988 and the PhD degree in 1992 both from the Universitat Autònoma de Barcelona (UAB). In 1994 he joined the "Departament d'Enginyeria Electrònica" (UAB) where he has been Full Professor of Electronics since 2007. He has been involved in different research activities including modelling and simulation of electron devices for high frequency applications, millimeter wave and THz generation systems, and the application of electromagnetic bandgaps to microwave and millimeter wave circuits. He is now very active in the field of metamaterials and their application to the miniaturization and optimization of microwave circuits and antennas. He is the head of the Microwave Engineering, Metamaterials and Antennas Group (GEMMA Group) at UAB, and director of CIMITEC, a research Center on Metamaterials supported by TECNIO (Generalitat de Catalunya).

Prof. Martín is a member of the IEEE Microwave Theory and Techniques Society (IEEE MTT-S). He is reviewer of the IEEE Transactions on Microwave Theory and Techniques and IEEE Microwave and Wireless Components Letters, among many other journals, and he serves as member of the Editorial Board of IET Microwaves, Antennas and Propagation and International Journal of RF and Microwave Computer-Aided Engineering.

Vicente E. Boria (S'91-A'99-SM'02) was born in Valencia, Spain, in 1970. He received his "Ingeniero de Telecomunicación" degree and the "Doctor Ingeniero de Telecomunicación" degree from the Universidad Politécnica de Valencia (UPV), Valencia, Spain, in 1993 and 1997, respectively. In 1993 he joined the "Departamento de Comunicaciones", Universidad Politécnica de Valencia, where he has been Full Professor since 2003. In 1995 and 1996, he was holding a Spanish Trainee position with the European Space Research and Technology Centre, European Space Agency (ESTEC-ESA), Noordwijk, The Netherlands, where he was involved in the area of EM analysis and design of passive waveguide devices. He has authored or co-authored 7 chapters in technical textbooks, 75 papers in refereed international technical journals, and over 150 papers in international conference proceedings. His current research interests are focused on the analysis and automated design of passive components, left-handed and periodic structures, as well as on the simulation and measurement of power effects in passive waveguide systems.

Dr. Boria is reviewer of the IEEE Transactions on Microwave Theory and Techniques, Proceeding of the IET (Microwaves, Antennas and Propagation) and IET Electronics Letters. Since 2013, he serves as Associate Editor of IEEE Microwave and Wireless Components Letters. He is also a member of the Technical Committees of the IEEE-MTT International Microwave Symposium and of the European Microwave Conference.